Polyaniline Fibers, Films, and Powders: X-ray Studies of Crystallinity and Stress-Induced Preferred Orientation

J. E. Fischer,*,† Q. Zhu,† X. Tang,‡ E. M. Scherr,‡ and A. G. MacDiarmid‡

Laboratory for Research on the Structure of Matter, University of Pennsylvania, Philadelphia, Pennsylvania 19104

V. B. Cajipe*

Institut des Matériaux des Nantes, CNRS–UMR 110, 2 rue de la Houssinière, 44072 Nantes Cedex 03, France

Received January 13, 1994®

ABSTRACT: Powder (*hk*0) and four-circle X-ray diffractometry are used to study the effects of hot-stretching on films and fibers of the emeraldine base form of polyaniline (EB-II). It is shown definitively that hot-stretching induces nucleation of new crystalline material rather than growth and/or orientation of pre-existing crystallites. The diffuse scattering from amorphous EB-II is dominated by short-range interchain correlations and develops preferred orientation in response to stretching but with a broader mosaic than the crystalline phase. For the maximally-stretched samples, the crystal fraction was determined by accounting for the different mosaic distributions of crystalline and amorphous phases, correcting for the mass of *N*-methylphenazolinium plasticizer and ruling out any significant contribution from NMP diffuse scattering to the amorphous EB-II profiles. Films stretched to $L/L_0 = 4.25$ contain no more than 4% crystalline material while fibers with $L/L_0 = 4.5$ are 24–30% crystalline. These fractional crystallinity values are significantly smaller than found for EB-II powder (60%). More importantly, these results have implications for models of electronic properties which invoke interchain interactions.

I. Introduction

From the synthetic standpoint, polyaniline is one of the most versatile conjugated polymers. The basic chain structure exists in three oxidation states,[1] various substitutions can be made to the backbone[2] or to the rings,[2,3] and most forms can be chemically doped.[4] Furthermore, many polyanilines can be prepared as powders,[5] films,[6] or fibers.[7] A detailed model of the electronic and magnetic properties has been developed from physical measurements on samples selected from this matrix of possibilities.[8]

Initial X-ray diffraction data on the emeraldine base form of polyaniline (EB-II prepared from *N*-methylphenazolinium or NMP solution) show this material to be partly crystalline, possibly to varying degrees in powders, films, and fibers.[9] Films and fibers can be stretch-oriented, which generally leads to property improvements thought to be associated with a closer realization of the intrinsic anisotropy.[10] This notion is supported by the observation that the X-ray diffraction after stretching is charactersitic of a "mosaic crystal" rather than a random powder; for thin films, the polymer chains in the crystalline phase are preferentially aligned along the stretch axis with a distribution full width at half-maximum (fwhm) of order 20°.[9] The property enhancements associated with stretch-orienting are, however, more modest in polyaniline[10] than usually obtained in other conjugated polymers, e.g., polyacetylene.[11] Thus a need exists for detailed characterization of the morphology and preferred orientation of stretch-aligned films and fibers. It is also important to separate the structural effects of morphology and orientation from the purely chemical consequences of substitutions and doping, to rationalize the range of properties observed in the whole family of polyanilines. A specific example is the proposed crossover from three-dimensional (3D) to quasi-one-dimensional (1D) behavior associated with increased average interchain separation in ring-substituted variants.[3]

Preliminary results suggest that the response of polyaniline to anisotropic strain is different from that of polyacetylene.[9] First of all, polyaniline is not intrinsically plastic and can only be stretch-aligned if the film or fiber contains a substantial amount of NMP, and then only by heating near the glass transition temperature defined by the NMP (ca. 140 °C).[6,7] This raises the question of the relative importance of thermal activation and anisotropic strain in the development of preferred chain orientation. A second difference vis-à-vis polyacetylene and other conjugated polymers is that the degree of crystallinity, i.e., the Bragg-scattering volume, apparently increases with increasing draw ratio; more typical behavior is the simple sharpening of the mosaic distribution of chain axes. Thus another important issue to resolve is whether hot-stretching of polyaniline films and fibers indeed induces nucleation and/or growth of crystalline regions or simply renders pre-existing crystallites more visible by concentrating a fixed total Bragg intensity into a smaller reciprocal space volume. A third set of issues has to do with the fact that the most crystalline materials (maximum draw ratio) still contain a substantial fraction of amorphous material, as revealed by diffuse X-ray scattering.[9] This suggests that the amorphous fraction could also exhibit preferred orientation, which must be taken into account in a proper determination of the fractional crystallinity. Of greater significance is the likelihood that chain alignment within the amorphous phase may also contribute to the enhancement of anisotropic mechanical and electronic properties by hot-stretching. This becomes all the more plausible in the light of the recent finding that the local order in amorphous undoped and HCl-doped type II polyaniline films resembles that found in the EB-II and ES-II crystalline structures, respectively, so that amorphous and crystalline phases cannot really be said to be clearly distinguishable.[12]

The main purpose of the work described in this paper is to obtain quantitative estimates for the relative amounts

* To whom correspondence should be addressed.
† Also: Department of Materials Science and Engineering.
‡ Also: Department of Chemistry.
® Abstract published in *Advance ACS Abstracts*, July 15, 1994.

0024-9297/94/2227-5094$04.50/0

of crystalline and amorphous phases in maximally-stretched EB-II films and fibers and to compare this with results obtained from random powders. This is done by a combination of four-circle and Debye–Scherrer X-ray diffractometry, using a data analysis procedure which differs from the usual pole figure texture determination in order to correctly account for different textures in the coexisting amorphous and crystalline phases. It is shown that hot-stretching induces the nucleation of new crystallites rather than simply aligning randomly oriented crystallites which existed before stretching. Also, the simultaneous crystallization and orientation are found to be solely due to anisotropic strain; thermal activation *per se* is unimportant. Furthermore, it is demonstrated that increasing the draw ratio of stretched fibers simply nucleates more crystallites with no increase in their size.

To correctly estimate the crystalline fraction, the orientation of the amorphous and the crystalline phases for both films and fibers is determined separately. This necessitates a discussion of the local structural origins of the diffuse scattering. The fractional crystallinity C is found to vary substantially among the three forms of polyaniline in the sequence C(powder) > C(fiber) > C(film). The latter value turns out to be surprisingly small, only a few percent. It is therefore obvious that interpretations of property measurements which rely implicitly or explicitly on long-range order must be seriously questioned. A byproduct of these studies is a confirmation of the basic features of the EB-II structural model for half-oxidized polyaniline developed by Pouget et al.[13]

II. Experiment and Analysis

The problem of determining fractional crystallinity in polymers was given a general treatment by Ruland in 1961.[14] His approach requires a knowledge of the structure factor $S(Q)$ for the amorphous and crystalline phases ($Q = 4\pi \sin\theta/\lambda$) and accounts for the fact that thermal diffuse scattering from the crystalline phase adds some diffuse intensity which must be corrected for to obtain the short-range-order scattering from the amorphous phase. In the introduction to this landmark paper, Ruland points out that all this detailed labor is unnecessary if one can calibrate the amorphous diffuse scattering against a known mass of purely amorphous material. One can further argue that if the crystalline fraction is small, then thermal diffuse scattering will only be a second-order correction to the amorphous diffuse profile. The emeraldine base form of polyaniline can be prepared as completely amorphous films or powders. C is also shown to be small enough to neglect thermal diffuse scattering. Thus the simplified method alluded to by Ruland may be applied here.

On the other hand, Ruland's analysis is limited to samples consisting of randomly-oriented crystallites in a completely nonoriented amorphous matrix. This condition is not satisified by stretched films and fibers, so a detailed texture study must be performed to correctly weight the mass-scaled amorphous contribution and to determine the "effective mass" of the crystalline part giving to Bragg peaks. In these materials, it is not sufficient to characterize the texture via the classical orientation function[15]

$$f = {}^3/_2(\langle\cos^2\sigma\rangle - 1) \qquad (1)$$

since the distribution of chain axes (especially in the amorphous phase) cannot be accurately represented by an average square cosine of the angle σ between the stretch axis and the polymer chain axes. Instead the actual distribution of chain axes in both crystal and amorphous phases can be determined and used to correctly weight the mass-scaled radial intensities. This approach has the added advantage that measurements of anisotropic physical properties (conductivity, Young's modulus, etc.) can be evaluated in terms of these actual chain axis distributions.

This combined procedure was carried out for emeraldine base (EB-II) films and fibers. Two diffractometers were used, both

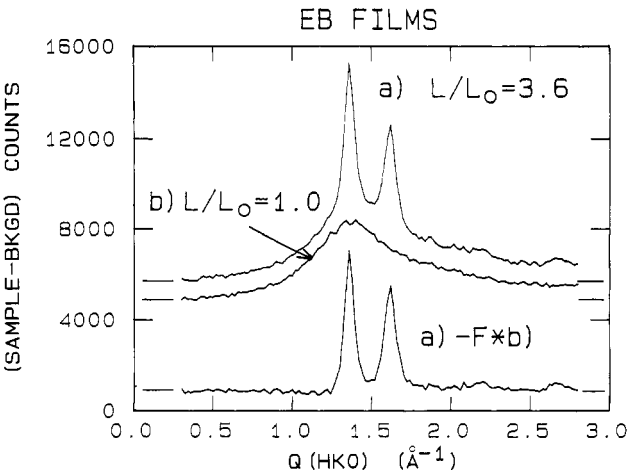

Figure 1. X-ray ($hk0$) scans from (a) stretched and (b) unstretched EB films; the bottom curve gives the difference.

based on 1.5 kW sealed-tube Cu anodes. Single fibers were studied with a curved "linear" detector[16] which gives the equivalent of an equatorial profile ($0 < 2\theta < 120°$) in a Debye–Scherrer (DS) experiment. Texture was studied using a home-made χ-circle attachment on a single-detector two-axis diffractometer; this instrument gives the analog of radial DS scans at different χ azimuths or azimuthal scans at fixed radius (or $|Q|$). Both instruments were equipped with graphite monochromators. All experiments were done in transmission geometry. Since polyaniline is a relatively poor scatterer, careful background subtraction was necessary for quantitative analysis. This requires that the sample absorption be negligible, to ensure that the background is the same with or without the sample in place. For all the film and fiber samples the transmission at $Q = 0$ was found to exceed 97%.

In the case of random powders, only the equatorial profiles are required. Diffuse scattering from glass or quartz capillaries would have complicated the analysis, so 1 mm diameter Ni tubes were fabricated by spot welding 0.0003 in. thick foil rolled onto a mandrel. The tubes of known length were weighed before and after loading with powder. These samples exhibited significant absorption of the X-ray beam, so the empty tube profile was corrected before subtraction such that the difference profile extrapolated smoothly to zero at low scattering angle. An experiment by Annis et al.[17] shows that small-angle scattering from large-scale density fluctuations can be safely neglected in our range of scattering angles.

As noted above, films and fibers of polyaniline contain a significant amount of NMP plasticizer which varies with stretch ratio. In principle, the NMP could contribute some parasitic diffuse scattering, and the NMP mass would surely affect the intensity normalization. A flat plate sample of NMP was prepared and its mass/area and scattering profile were measured. By this procedure it was confirmed that, for the NMP levels present in our samples, diffuse scattering from the NMP is negligible. The measured masses were also corrected for NMP content by performing thermogravimetric analysis (TGA) after the diffraction experiments to determine the exact amount in each sample from the weight loss centered at 150 °C. This was impossible on individual fibers so data from comparable fiber bundles were used to make the mass correction.

Figure 1 sets the stage for what follows. The top curve is a background-substracted ($hk0$) (equatorial) scan of an EB film stretch-oriented to a draw ratio $L/L_0 = 3.6$. The prominent peaks are identified as (110) and (200) Bragg reflections of the orthorhombic EB-II structure.[12] There is also considerable diffuse scattering in the same Q range. The middle curve, a similar scan from unstretched film, shows no evidence of Bragg peaks but reveals diffuse scattering that is most intense in the Q range of the two strong ($hk0$) peaks in the stretched film. The bottom curve is obtained by subtracting the middle profile, appropriately scaled, from the top one. The stretched and unstretched films have mass/area m_S and m_U, respectively (S and U denoting stretched and unstretched), and the latter profile must be

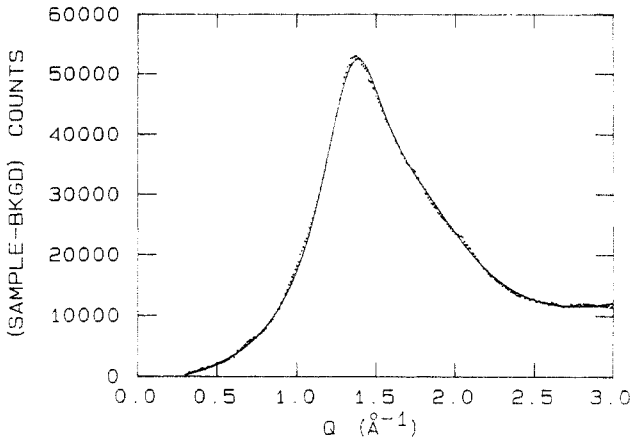

Figure 2. Diffuse scattering from an assembly of unstretched EB films (dots); the solid curve represents a fit using an *ad hoc* function (see text).

multiplied by a factor F to yield a difference spectrum with a flat zero baseline and devoid of diffuse scattering. Thus, *if there were no preferred orientation*, the stretched film would consist of Fm_U mg/mm² amorphous and $(m_S - Fm_U)$ mg/mm² crystalline material. Note however that if the crystalline phase were highly oriented while the amorphous phase were completely random in χ, the mass of crystalline material and hence the fractional crystallinity would be grossly overestimated.

In principle, both the amorphous and crystalline scattering, as recorded in a radial scan at some appropriate azimuth, will be enhanced by preferred orientation relative to the intensity expected from an equal mass of a perfectly random powder. Conversely, the mass responsible for a given radial intensity is reduced by preferred orientation relative to the mass of powder giving the same intensity. These reduction factors can be determined from the analysis described below and are defined as follows. For a range of values spanning at least one quadrant of the χ plane, the radial peak intensity of an appropriate crystal Bragg reflection and the Q-integrated diffuse scattering from the amorphous phase are determined. These are both integrated over χ and normalized to the integrated intensity of a powder sample giving the same peak intensity. The reduction factors R_a and R_c are used to obtain the "effective masses" of amorphous and crystalline fractions R_aFm_U and $R_c(m_S = Fm_U)$ mg/mm², repectively. Fractional crystallinity is then defined as

$$C = R_c(m_S - Fm_U)/[R_c(m_S - Fm_U) + R_aFm_U] \qquad (2)$$

The absolute accuracy is limited mainly by the term in parentheses, which is typically a small difference between two comparable magnitudes; m_S and m_U are comparably small to ensure negligible absorption, and F is typically about 0.5. The accuracy also depends on the parameters of the experiment; in the results presented below, it varies from ±0.03 to ±0.07.

Preparation of the powders, films, and fibers of EB-II polyaniline used in the present study and the subsequent hot-stretching of the latter two are described in detail elsewhere.[5-7]

III. Results and Discussion

Diffuse Scattering from Unstretched Films. As a prelude to the texture analysis described above, a universal description of the diffuse scattering from amorphous EB-II, which could then be used to analyze composite profiles versus draw ratio or azimuth, was sought. This was done by measuring a very thick assembly of folded unstretched films, using reflection rather than transmission to increase the scattering volume. Figure 2 shows a portion of the profile from a 0.45 mg/mm² assembly (≈50 times thicker than our typical film samples). The measured profile after background subtraction (dots) is typical of a liquid or glass with short-range correlations; the intensity tends to zero at $Q = 0$, rises to a single asymmetric peak, and asymptotes to a constant value associated in part with incoherent (Compton) scattering. The smooth curve is a least-squares fit to an *ad hoc* function consisting of the sum of two Lorentzians to describe the asymmetry and a quadratic $A + BQ + CQ^2$ to reproduce the nonzero high-Q asymptote. This algorithm gives an excellent description of the data in the range $0.3 < Q < 3.0$ Å⁻¹. The fitted Lorentzians are centered at 1.34 and 1.69 Å⁻¹, very close to the positions of the (110) and (200) Bragg peaks. The d values of these ($hk0$)s (4.69 and 3.72 Å, respectively) represent the two shortest interchain distances in the rectangular (a,b) basal cell. There is of course no one-to-one correspondence between diffuse peaks and interatomic distances in any but the simplest glasses or liquids. However, the results of the fit do suggest that amorphous EB retains the short-range interchain correlations of the crystal and that in this Q range the diffuse scattering is dominated by interchain rather than intrachain short-range order. This statement is supported by the amorphography study of unstretched EB-II film[12] which attributed the radial distribution function peaks at distances between 3.4 and 7 Å to interchain correlations. These correlations are limited in range by the intrachain conformational defects in amorphous EB-II, i.e., the distribution of values for δ (the zigzag ring–N–ring angle, ≈130°) and ϕ (the C_6 ring torsion angle relative to the plane of the N atoms, ≈30°); these two main degrees of freedom of the polyaniline chain control the chain packing by steric interactions.

Our initial plan was to use the above algorithm multiplied by an overall amplitude, in combination with appropriate representations of Bragg peaks, to fit composite radial scans of films and fibers versus draw ratio or azimuth. This would establish a simple measure of the radial peak diffuse intensity versus χ for determining the distribution of chain axes or versus draw ratio for assessing the evolution of crystallinity with stretching. Two preconditions are that the amorphous contribution in stretched films and fibers be dominated by interchain short-range correlations (i.e., "($hk0$)-type" diffuse scattering) independent of χ and that the short-range interchain correlations be independent of draw ratio. It subsequently became clear that neither of these preconditions is precisely satisfied; to optimize the combined (crystal + amorphous) fits, the parameters of the diffuse scattering algorithm were allowed to vary slightly with χ and/or draw ratio. This complicates the problem of characterizing the preferred orientation of the amorphous phase but also suggests that a proper analysis of short-range order versus orientation and/or draw ratio via the radial distribution function would be worthwhile.

EB-II Fibers. Figure 3 shows equatorial profiles of individual fibers with draw ratios L/L_0 = "1", 3.1, and 4.5. The fiber cross-sections are roughly rectangular (50 × 100 μm² for unstretched material) and the mass/length varies from 0.036 to 0.016 mg/mm as L/L_0 increases from "1" to 4.5. The fibers were rotated about their axes during data collection on the curved detector diffractometer to improve the powder averaging (typically 3–8 h per profile). Background-subtracted data are represented by dots, while the solid curve is a fit to the sum of an amorphous line shape as described above, plus Gaussians representing crystalline Bragg peaks. The (110) and (200) reflections occur at the same d values as the two strong peaks in a stretched film (Figure 1).

It is quite evident that the relative strength of amorphous diffuse scattering decreases with increasing L/L_0, suggesting qualitatively that the crystal fraction increases with L/L_0 (this point is quantified using the texture results

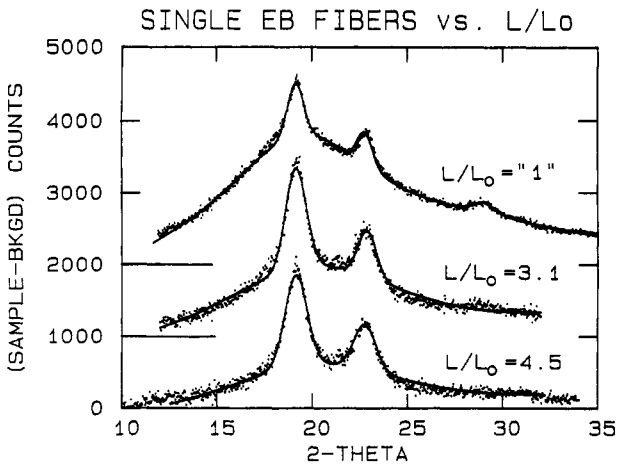

Figure 3. X-ray powder diffraction data from single EB-II fibers of various draw ratios obtained using a curved position-sensitive detector (λ = 1.542 Å).

below). Indeed, stress-induced crystallization is known to occur in some nonconjugated polymers.[18] The fitted widths of the Bragg peaks, however, do not vary with L/L_0; the crystallite size in the (a,b) plane (inferred from the Scherrer formula) remains essentially constant at ≈100 Å. Thus the increase in the crystallinity with increasing L/L_0 is due to nucleation of new crystallites rather than growth of pre-existing ones. The nominally unstretched fiber (top curve) exhibits small but readily observable crystalline peaks. Unlike cast films with no observable crystal fraction (cf. Figure 2), it is difficult to totally avoid stretching the fibers as they are drawn from the precursor liquid.

Some important qualitative information about stretch-induced preferred orientation is also provided by Figure 3. First, the small crystalline fraction of the "unstretched" fiber (top curve) diffracts like a powder since the (211) at 29° is clearly observed in an equatorial scan. This peak's diminishing in intensity with increasing L/L_0 (the bottom curve for L/L_0 = 4.5 reveals only (hk0) reflections) may be taken as a signature of the stretch alignment of the crystalline phase. Second, the optimized least-squares fit in Figure 3 required releasing both the Lorentzian and quadratic parameters of the amorphous line shape from the values obtained in the fit to the thick film data (Figure 2). This indicates that the short-range order changes subtly with increasing L/L_0, which is not surprising since, as pointed out by Laridjani et al.[12], the chains in amorphous polyaniline contain imperfections which conceivably evolve with applied stress to an extent determined by the magnitude of the induced strain. These questions could in principle be addressed by subtracting off the Bragg peaks and performing a radial distribution function analysis on the remaining diffuse scattering.

A texture study was performed on an assembly of 18 fibers drawn to L/L_0 values in the range 3.5–4.2 by performing radial Q scans as a function of the angle χ. The fibers were mounted side-by-side over a 6 mm diameter aperture, spaced in such a way that the 1 mm width of the X-ray beam resulted in approximately constant scattering volume versus χ. Figure 4 shows data and fits for χ = 0, 15, 70, and 90°, the first and last of these corresponding to equatorial (hk0) and meridional (00l) azimuths, respectively. At χ = 0°, the crystal (110) and (200) peaks are superposed on a strong diffuse peak. At 15° the (hk0)s and the diffuse scattering are weaker, and a new feature at 2.05 Å^{-1} can be unambiguously identified as the (211) reflection of EB-II.[13] These trends continue with increasing χ until at 70° no (hk0) or (hkl) reflections are detectable

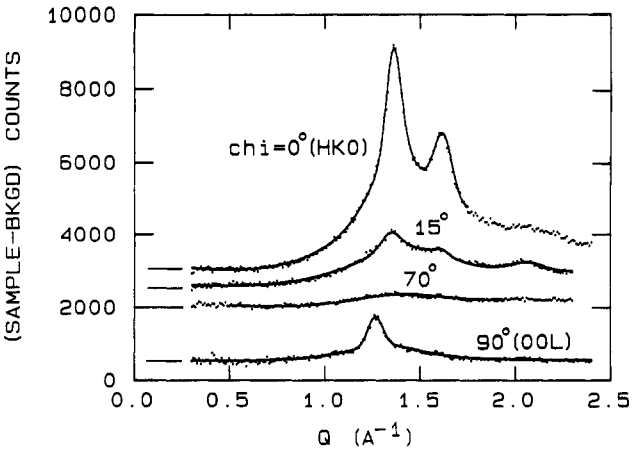

Figure 4. Q scans from the 18 EB-II fiber "picket fence" sample at χ = 0, 15, 70, and 90°.

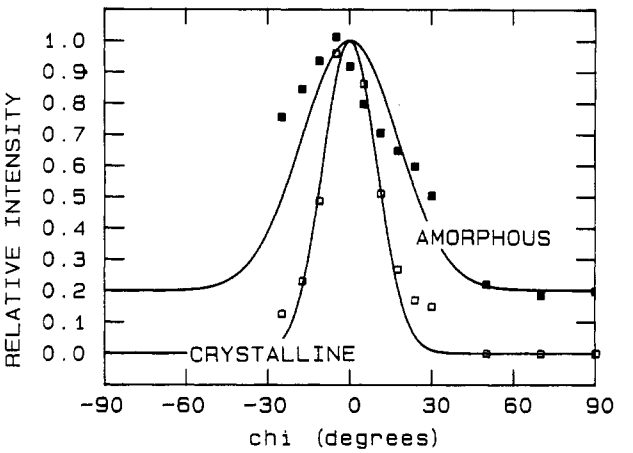

Figure 5. Textures (intensity versus χ) of the amorphous and crystalline components of the 18-fiber sample.

and the diffuse scattering is considerably weaker. Finally, at 90° a reflection which indexes as the (002) of EB-II is observed atop the now weak diffuse scattering. The progression of Bragg intensities with χ clearly reveals the preferred orientation of the crystalline phase. But these four profiles show that the chains in the amorphous phase are also preferentially aligned along the stretch axis. The onset of strong "(hk0)" amorphous scattering well below the first Bragg peak is quite evident in the 0° profile but is barely visible in the 90° one.

Several radial scans were made at other χ values and each profile in the set was modeled by a superposition of Gaussian Bragg peaks and diffuse scattering (e.g., the solid curves in Figure 4). The amorphous profile has the same qualitative Q dependence over the entire χ range, but significantly better overall fits were again obtained by allowing the parameters of the amorphous profile to vary with χ. This weak orientation dependence most probably follows from the conformational defects within the chains "healing" progressively as a function of the chain alignment.

The textures of the crystal and amorphous phases were determined from the χ dependences of the fitted (110) amplitudes and integrated diffuse intensities ($0.5 < Q < 2.5$ Å^{-1}), respectively. These are shown in Figure 5 as open and filled squares, respectively, both normalized to unity at the maxima. The solid curves are Gaussian fits. For the crystalline phase, the stretch-induced texture is well described by a Gaussian distribution of chain axes with a full width at half-maximum (fwhm) of 20° (corrected for finite resolution), a small part of which could be from

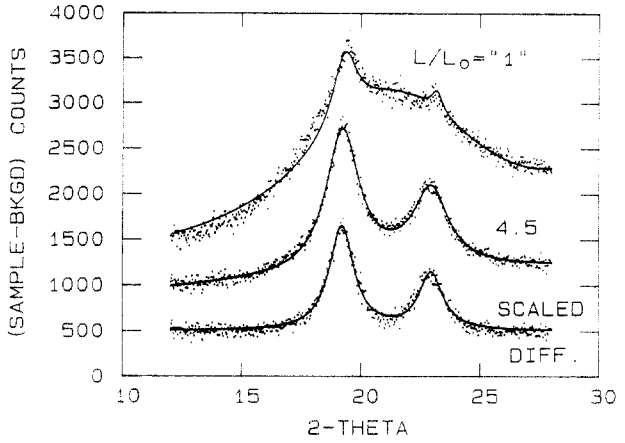

Figure 6. Obtaining the scale factor F for stretched fibers by appropriate subtraction of intensity from an unstretched fiber of known mass/length m_U (see text).

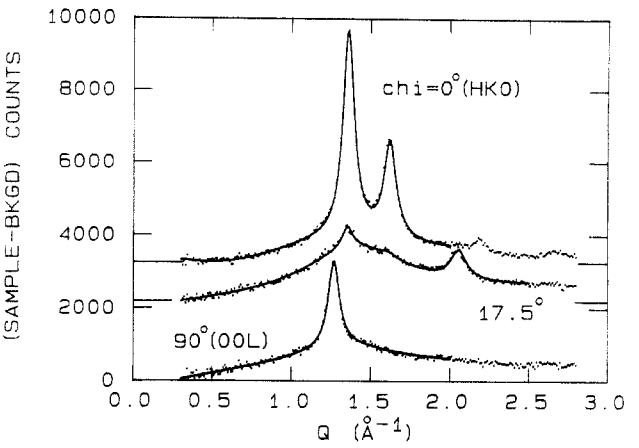

Figure 7. Q scans at three χ values for a stretched EB-II film with $L/L_0 = 4.25$.

alignment errors among individual fibers. Since there is no detectable ($hk0$) intensity at $\chi = 90°$, all of the crystalline material is accounted for in the Gaussian distribution. A direct measurement of the crystal mosaic from a χ scan at fixed $Q(110)$ is consistent with this more tedious determination. Of greater interest is the obvious preferred orientation exhibited by the amorphous phase. Having argued that the diffuse scattering is dominated by short-range interchain correlations, the χ dependence of this scattering shows that the chains in the amorphous phase are also preferentially aligned along the stretch axis. Unlike the crystal phase, however, the amorphous "($hk0$)" scattering is not zero on the meridian, indicating that a significant fraction does not respond to stretch alignment. The overall texture of the amorphous phase is represented fairly well in Figure 5 by a constant plus a Gaussian with 42° fwhm, about twice as broad as the crystal fwhm. The relative areas of these two components are about equal. In maximally-stretched fibers, half the amorphous phase is random while the chains in the other half are oriented in the same direction as the chains in the crystalline phase, albeit more weakly. An analogous partition of random and oriented *crystalline* fractions occurs in thick polyacetylene films which are aligned during polymerization by a nematic liquid crystal substrate.[19]

The parameters characterizing the textures in Figure 5 were used to determine the mass reduction factors $R_a = 0.40$ and $R_c = 0.13$ for this set of fibers. Figure 6 describes the determination of F from the difference between background-subtracted DS profiles of two fibers with $L/L_0 = 4.5$ and (nominally) 1.0 and mass/length values of 15.6 and 36.5 μg/mm, respectively (corrected for NMP). The unstretched fiber (top curve) was counted for a longer time than the stretched one (middle curve) to obtain comparable statistics. This unstretched fiber shows considerably less Bragg intensity than the one in Figure 3. The fits to these two profiles (solid curves) both include the amorphous profile and the Bragg peaks. The bottom curve is the difference between the top curve and F times the middle one. F is determined by trial and error, the criterion being that the baseline above and below the two Bragg peaks have the same average value (close to zero). This is determined numerically by summing the first and last 50 data points (the profiles shown represent 525 channels of the 1-D detector). The sum of the first 50 points is only weakly dependent on F, indicating that the background subtraction was done correctly. In contrast, the sum of the last 50 points is very sensitive to F because the amorphous contribution has a nonzero asymptote at large angle whereas the correct, purely crystalline difference spectrum should be zero in this range (assuming no detectable incoherent scattering from the crystalline phase). An independent check on F is obtained by fitting the difference profile with no background of diffuse line shape; since this yields a good fit (bottom solid curve), the difference profile contains only the two Bragg peaks of the crystalline phase. For the data shown in Figure 6, $F = 0.312$ with a conservative error estimate of ± 0.0005. Thus from eq 2 and accounting for different counting times and the weak $L/L_0 = 1$ Bragg intensity, the fractional crystallinity in EB-II fibers stretched to L/L_0 in the range 3.5–4.5 is $C = 0.27 \pm 0.03$. Fibers with smaller L/L_0 undoubtedly exhibit smaller C values (as suggested by Figure 3).

Stretched EB-II Film. Radial Q scans at three χ values are shown in Figure 7 for an EB-II film drawn to $L/L_0 = 4.2$ (dots are the background-subtracted data, and solid curves are fits including amorphous and crystalline contributions). The results are qualitatively similar to those of Figure 4 for stretch-aligned fibers, a notable difference being that the diffuse scattering remains stronger as χ moves from the equator to the meridian. The 0° profile is again dominated by intense (110) and (200) crystal peaks at 1.35 and 1.61 Å^{-1}, respectively; also visible are weaker peaks near 2.2 and 2.7 Å^{-1} which may be indexed as (020) and (310) in the EB-II model (these features were not included in the fit). At $\chi = 17.5°$, all ($hk0$) intensities are greatly reduced but the diffuse scattering is largely unaffected; as in the case of the fibers, a Bragg peak is detected at 2.04 Å^{-1} with both $|Q|$ and χ consistent with the EB-II (211) reflection. At $\chi = 90°$ the EB-II (002) at 1.26 Å^{-1} is clearly observed as well as diffuse scattering with intensity and profile similar to that at $\chi = 0°$. These observations indicate qualitatively that the crystalline phase is about as well aligned as it was in the fibers, but the amorphous phase in the film is more nearly random. The Scherrer formula again yields crystallite sizes of order 100 Å from both ($hk0$) and ($00l$) widths.

Figure 8 shows the preferred orientation of amorphous and crystalline phases in the $L/L_0 = 4.2$ film. A χ scan of the (110) reflection (open squares) yields a Gaussian profile with 20° fwhm which accounts for all the Bragg intensity, while the χ dependence of the integrated diffuse intensity (filled squares) is adequately described by a constant plus a broad Gaussian. These deductions are qualitatively the same as for fibers drawn to comparable L/L_0 (Figure 5) but there are important quantitative differences. The film exhibits a much greater fraction of unoriented amorphous material, and the width of the oriented part is considerably larger, ≈80° versus ≈40° fwhm. It thus appears that the

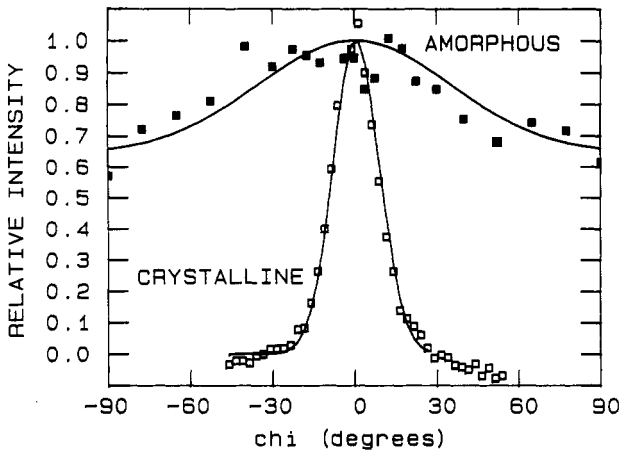

Figure 8. Textures of the amorphous and crystalline phases of the $L/L_0 = 4.25$ stretched EB-II film.

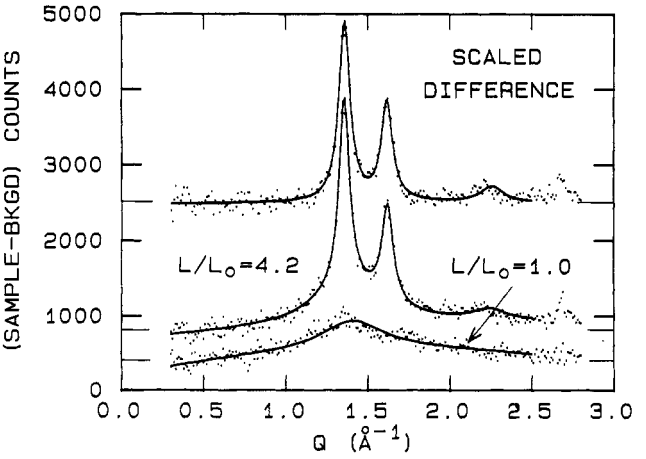

Figure 9. Obtaining the scale factor F for the $L/L_0 = 4.25$ film sample.

crystalline material is oriented to about the same extent (for a given draw ratio) in films and fibers, whereas the chains in the amorphous part of the film are harder to align than those in the fibers. It is also clear that for films, radial scans give a misleading impression of the degree of crystallinity; the reduction factors from Figure 8 are 0.82 and 0.047 for the amorphous and crystalline phases, respectively.

The fractional crystallinity for the film is determined as shown in Figure 9. Here the stretched and unstretched films were counted for equal times, and the mass/area values differed by only 10%. Thus the raw data indicate directly that most of the mass of the stretched film is in fact amorphous. Coupled with the large difference in reduction factors imposed by the much different textures, the crystal fraction is small indeed. The film masses are quite accurate since the NMP content of the actual X-ray samples were determined by TGA. The profile scaling factor F is very conservatively determined as 1.04 ± 0.01 using criteria described above. In particular, the fit to the scaled difference profile in Figure 9 was performed with floating background parameters which, when optimized, gave negligible integrated intensity. This again shows that the scaled difference yields only Bragg scattering; thus F is correctly determined. Using eq 2 C is calculated to be 0.02 ± 0.02; thus the *upper bound* for the crystalline fraction in maximally-stretched films is only 0.04.

To isolate the role of heating in chain alignment during drawing, the unstretched film shown in Figure 1 was annealed for 15 h at 120 °C in dynamic vacuum. This treatment had no detectable effect on the diffraction

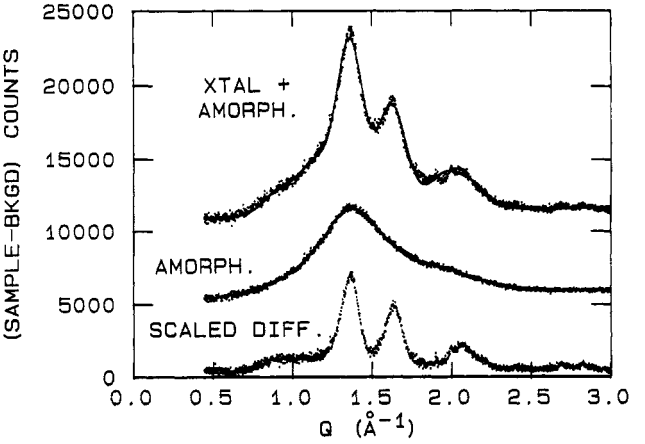

Figure 10. Data and fits for amorphous and partially crystalline EB-II powder and the scaled difference.

profile. Since the time involved in the hot-stretching process is orders of amgnitude smaller, it may be concluded that thermal processes *per se* play no role in the alignment or crystallization and that high temperature is only necessary to render the material plastic. An upper bound on the fraction of pre-existing crystalline material in unstretched films may be obtained as follows. There are no detectable Bragg peaks in the profile shown in Figure 2, which was counted with 10 times better statistics than Figure 9 on a film "sandwich" 50 times more massive. These factors enhance the sensitivity to crystalline material by about 500 times as compared to Figure 9. On the other hand, for an unstretched film $R_c = R_a = 1$ so the sensitivity to Bragg peaks decreases by a factor of 20 as compared to Figure 9. Thus a Bragg peak in the Figure 2 profile *with the same radial intensity as from the stretched film in Figure 9* (relative to the diffuse scattering) is attributed to a crystal fraction of order 25 times smaller. With a conservative estimate of 0.1 on this relative intensity, the unstretched film thus contains at most $C = 0.0002$ (0.02%) crystalline material.

EB-II Powders. Figure 10 shows background-subtracted data and fits for measured quantities of amorphous and partially crystalline EB-II powder. The latter is referred to as THF/NMP extract in ref 13 and is converted into completely amorphous material by HCl doping into so-called ES-II powder and dedoping. Since there is no texture involved in either the crystalline or amorphous contributions, C is determined simply by scaling the diffuse scattering to the sample mass. Unlike the results for films and fibers, the diffuse scattering profile of amorphous EB-II powder is found to be drastically different before and after the doping/dedoping process. Subtraction of the scaled amorphous profile (Figure 10, middle) from the mixed-phase profile (Figure 10, top) does not produce a purely crystalline pattern (Figure 10, bottom) in contrast to Figures 6 and 9 for fibers and films, respectively. Thus, the short-range correlations in amorphous EB-II are different before and after doping/dedoping. This had been observed in the case of film samples as well, and the interpretation that has been given is that the doping/dedoping process is accompanied by variations in ring tilt ϕ and zigzag angle δ which then lead to a large distribution of intrachain distances that yield a local interchain order intermediate between those of as-cast EB-II and ES-II films.[12]

C for powders can nevertheless be estimated by integrating separately the fitted diffuse scattering from the two samples. The fractional crystallinity is found to be $60 \pm 8\%$, substantially greater than the fiber value and

vastly greater than the film value. It is noteworthy that a slightly smaller fraction (50%) is obtained when the crystalline and amorphous integrated intensities are not normalized by the two phases' respective mass densities.[13] A point that might be reconsidered in this connection would be the possibility that C for powders varies with the molecular weight distribution of the precursor monomer; this could then explain the dependence of the doped materials' conductivity on the latter.[20,21]

IV. Conclusion

The main conclusion of the present study is that the fractional crystallinity of EB-II polyaniline is strongly dependent on the sample morphology; a concomitant finding is that the amorphous component of EB-II films and fibers can be oriented by stretching. While hot-stretching films and fibers fourfold yields 4 and 30% crystalline material, respectively, direct polymerization of powders leads to a maximal 60% crystallinity.

The effect of stretching a film or fiber may be understood by assuming an initially 100% amorphous sample, i.e., a mass of completely nonaligned chains. With the application of stress a fraction X of the chains responds by orienting themselves along the stretch axis so the sample becomes textured. The strains induced in these regions presumably modify the conformational defects[12] and are nonuniform, being expectedly larger for the better-aligned chains. A smaller fraction Y may thus be envisioned to have "critically" healed imperfections and form domains of more closely-packed chains, whence the appearance of long-range spatial correlations and tighter orientation, i.e., a crystalline phase with improved mosaicity. The fractions Y and X are not the same for films and fibers of similar L/L_0 simply because the strain anisotropy is governed by the aspect ratio, which is evidently very different in the two cases. By the same token, while the crystalline phase in films and fibers exhibits the same degree of orientation, the amorphous material in film is less responsive to stretch alignment. It would be interesting to determine how the crystalline and amorphous textures evolve with L/L_0 in the two types of material.

Given that both crystalline and amorphous phases of stretched films and fibers are oriented, with the former fraction being much smaller than the latter, the degree of orientation of the average chain may be calculated by weighting the mosaic associated with each part. This is the kind of information that should be used to interpret the anisotropy of measured quantities which depend only on the properties of individual chains (e.g., Raman vibrational modes). For quantities which depend on both the properties of single chains and the short-range interchain coupling, the same anisotropy analysis applies since the local order in amorphous EB-II very closely resembles that in crystalline EB-II. The oriented amorphous fraction may thus be expected to enhance the anisotropy of the mechanical properties, for example; such a contribution may be partly responsible for the greater tensile strength of drawn fibers as compared to similarly stretched films.[21]

As alluded to earlier, the conductivity of polyaniline does not increase as dramatically with stretching as that of polyacetylene.[10,11] Oriented ES-II which results from HCl doping of EB-II film has been proposed to represent a class of quasi-1D disordered conductors formed by "metallic" bundles of coupled parallel chains in which the electronic states are extended in 3D.[22] It has recently been pointed out by Pouget et al.[23] that such a model agrees well with the description of stretched polyaniline material as consisting of crystalline domains embedded in an amorphous matrix: the continuous loss of order between these domains and amorphous regions may be thought to be accompanied by a weakening of the electronic wave functions' extension (3D), i.e., eventual localization (1D). The results presented above give good estimates for the mass fraction of crystalline bundles in maximally-stretched EB-II films and fibers; although these values may be expected to increase slightly with HCl doping, their small magnitude explains the weak stretch enhancement of the obtained ES-II materials' conductivity. Also, the finding that the amorphous phase is characterized by a rather broad mosaic provides a mechanism for the gradual loss of long-range order in addition to the spatial correlations' becoming progressively limited as one moves away from the crystalline bundles.

The other highlights of the present work may be related to the amorphography results of Laridjani et al.[12] Amorphous polyaniline contains very little crystalline material so that hot-stretching necessarily involves nucleation rather than growth; the simultaneous crystallization and orientation are solely due to the anisotropic strains which transform the chain imperfections. Increasing the draw ratio simply nucleates more crystallites with no increase in their size; the remaining fraction of amorphous material is substantial but is presumably increasingly oriented. The degree of crystallinity achievable in EB-II films and fibers thus appears to be limited by the intrachain disorder of the starting polymer and the ability of uniaxial stretching to apply the stress needed to heal such throughout the sample volume.

Finally, it is worth mentioning that our four circle diffractometer fiber and film data confirm the EB-II structural model proposed by Pouget et al. on the basis of powder diffraction.[13]

Acknowledgment. This research was supported by the NSF MRL Program (Grant No. DMR91-20668) and DOE Grant DEFG02-87ER45254. We thank A. R. McGhie for performing the thermogravimetric analysis.

References and Notes

(1) Epstein, A. J.; MacDiarmid, A. G. In *Proceedings, NATO Advanced Study Institute Spetses, Greece*; Metzger, R., Ed.; Plenum Press: New York, 1989.
(2) MacDiarmid, A. G.; Epstein, A. J. *Faraday Discuss. Chem. Soc.* **1989**, *88*, 317.
(3) See, for example: (a) Wang, Z. H.; Javadi, H. H. S.; Ray, A.; MacDiarmid, A. G.; Epstein, A. J. *Phys. Rev. B.* **1990**, *42*, 5411. (b) Wang, Z. H.; Javadi, H. H. S.; MacDiarmid, A. G.; Epstein, A. J. *Phys. Rev. B.* **1990**, *43*, 4373. (c) Pouget, J. P.; Zhao, S. L.; Wang, S. H.; Oblakowski, Z.; Epstein, A. J.; Manohar, S. K.; Wiesinger, J. M.; MacDiarmid, A. G.; Hsu, C. H. In press.
(4) See, for example: (a) MacDiarmid, A. G.; Chiang, J. C.; Richter, A. F.; Epstein, A. J. *Synth. Met.* **1987**, *18*, 285. (b) Jozefowicz, M. E.; Epstein, A. J.; Tang, X.; MacDiarmid, A. G. In press.
(5) MacDiarmid, A. G.; Chiang, J. C.; Richter, A. F.; Somasiri, N. L. D.; Epstein, A. J. In *Conducting Polymers*; Alcacer, L., Ed.; D. Reidel Publishing Co.: Dordrecht, The Netherlands, 1987; p 105.
(6) Angelopoulos, M.; Asturias, G. S.; Ermer, S. P.; Ray, A.; Scherr, E. M.; Akhtar, M.; Kiss, Z.; Epstein, A. J. *Mol. Cryst. Liq. Cryst.* **1988**, *160*, 151. Cromack, K. R.; Jozefowicz, M. E.; Ginder, J. M.; Epstein, A. J.; McCall, R. P.; Du, G.; Leng, J. M.; Kim, K.; Li, C.; Wang, Z. H.; Druy, M. A.; Glatkowski, P. J.; Scherr, E. M.; MacDiarmid, A. G. *Macromolecules* **1991**, *24*, 4157.
(7) Tang, X.; Scherr, E. M.; MacDiarmid, A. G.; Epstein, A. J. *Bull. Am. Phys. Soc.* **1989**, *34*, 583.
(8) Epstein, A. J.; MacDiarmid, A. G. In *Frontiers of Polymer Research*; Prasad, P. N., Nigam, J. K., Eds.; Plenum Press: New York, 1991; p 339 and references therein.
(9) Fischer, J. E.; Tang, X.; Scherrer, E. M.; Cajipe, V. B.; MacDiarmid, A. G. *Synth. Met.* **1991**, *41–43*, 41.

(10) Epstein, A. J.; MacDiarmid, A. G. *Synth. Met.* **1991**, *41–43*, 601 and references therein.
(11) Tsukamoto, J.; Takahashi, A.; Kawasaki, K. *Jpn. J. Appl. Phys.* **1990**, *29* (1), 125.
(12) Laridjani, M.; Pouget, J. P.; Scherr, E. M.; McDiarmid, A. G.; Jozefowicz, M.; Epstein, A. J. *Macromolecules* **1992**, *25*, 4106.
(13) Pouget, J. P.; Josefowicz, M. E.; Epstein, A. J.; Tang, X.; MacDiarmid, A. G. *Macromolecules* **1991**, *24*, 779. Jozefowicz, M. E.; Laversanne, R.; Javadi, H. H. S.; Epstein, A. J.; Pouget, J. P.; Tang, X.; MacDiarmid, A. G. *Phys. Rev. B.* **1989**, *39*, 12958.
(14) See: Kakudo, M.; Kasai, N. *X-Ray Diffraction by Polymers*; Kodansha Ltd. (Tokyo) and Elsevier Publishing Co. (Amsterdam, The Netherlands), 1972.
(15) Ward, I. M. *Structure and Properties of Oriented Polymers*; John Wiley and Sons: New York, 1975.
(16) INEL, Les Ulis, France.
(17) Annis, B. K.; Lin, J. S.; Scherr, E. M.; MacDiarmid, A. G. *Macromolecules* **1992**, *25*, 429.
(18) Stein, R. S.; Misra, A. *J. Polym. Sci., Polym. Phys. Ed.* **1979**, *17*, 235.
(19) Coustel, N.; Foxonet, N.; Ribet, J. L.; Bernier, P.; Fischer, J. E. *Macromolecules* **1991**, *24*, 5867.
(20) Scherr, E. M.; MacDiarmid, A. G.; Manohar, S. K.; Masters, J. G.; Sun, Y.; Tang, X.; Druy, M. A.; Glatkowski, P. J.; Cajipe, V. B.; Fischer, J. E.; Cromack, K. R.; Jozefowicz, M. E.; Ginder, J. M.; McCall, R. P.; Epstein, A. J. *Synth. Met.* **1991**, *41–43*, 735.
(21) MacDiarmid, A. G.; Epstein, A. J. *Mater. Res. Soc. Symp. Proc.* **1990**, *173*, 283.
(22) Wang, Z. H.; Li, C.; Scherr, E. M.; MacDiarmid, A. G.; Epstein, A. J. *Phys. Rev. Lett.* **1991**, *66*, 1745.
(23) Pouget, J. P.; Laridjani, M.; Jozefowicz, M. E.; Epstein, A. J.; Scherr, E. M.; MacDiarmid, A. G. *Mater. Res. Soc. Symp. Proc.* **1992**, *247*, 589.